Chapter 3

Relating changes in interval slowness to residual slowness

3.1 Introduction and overview

The previous chapter provides a method for measuring residual slowness (or velocity) which measures moveout or discrepancy in position versus offset of the images of reflectors after prestack depth migration. To make these measurable residual slownesses useful for interval-velocity analysis requires relating them to changes in an interval-slowness model. This chapter develops an operator that relates the unknown but physically relevant interval slownesses to residual slownesses that can be measured.

Loinger (1983) and Toldi (1985) described linear relations between laterally varying interval slownesses and observed laterally varying stacking slownesses for horizontal reflectors. Fowler (1988) extended Toldi's work and derived a linear relation between prestack time-migration slownesses or DMO-corrected stacking slownesses and interval slownesses for arbitrary structure. I extend the previous work and build an operator that relates residual slowness, measured after prestack depth migration, to changes in the interval-slowness model used for prestack depth migration. In the words of Fowler (1988) the operator I build, like the aforementioned operators, is a filtered traveltime-tomography operator. They are "tomography" operators because they involve a traveltime-tomography calculation. The "filter" converts the changes in traveltime to changes in stacking slowness, prestack time-migration slowness, or residual slowness.

The advantage of using prestack depth migration and residual prestack migration for

velocity analysis rather than using DMO-corrected stacking slownesses or prestack time-migration slownesses is two-fold. First, depth migration is needed to position events properly. It is easier to compute the correct location of a migrated event as a residual correction to a prestack depth-migrated image than find its location from a stacked image or time-migrated image. More importantly, since the estimation process is iterative and large changes to the interval-slowness model may accumulate, it is important to incorporate the effects of changes in the interval slowness into the background model as the iterations proceed. Depth migration gives proper common-reflection-point gathering, moveout correction, and event positioning in a laterally varying velocity model. Methods that rely on NMO, NMO and DMO, or time migration can't fully remove the effects of a laterally varying background velocity model because they use constant-velocity kinematics to focus and position events.

As discussed in Chapters 1 and 2, it is desirable to estimate residual slownesses for fixed reflection events, rather than fixed points in depth. The tomography calculations carried out to build the operator have to be performed for fixed points in depth. Therefore, the operator is built in two parts. The first part (section 3.2) finds a relation between changes in the interval-slowness model and changes in both the residual slowness and apparent position of a fixed point in depth using traveltime tomography. The second part (section 3.3), takes the changes in residual slowness for fixed depth points and converts them to changes in residual slowness for fixed events. To do this, I find the new depth locations of all fixed events and interpolate their residual slownesses from the residual slownesses of the underlying fixed depth points. This calculation employs the zero-offset part of residual prestack migration saved from Chapter 2 to model the movement of reflection events.

3.2 Reflector tomography for fixed depth points

There are three components to the first part of the tomographic operator. First, using traveltime tomography, I find the changes in traveltimes to fixed points in depth due to changes in the interval-slowness model. Second, a change in the traveltime to a fixed depth point implies that the image of any reflector present there must move. The implied reflector movement means that the fixed depth point displays the image of a different reflector. Using the kinematics of residual migration from Chapter 2, compute the location of the event that moves to the fixed depth point as the model changes. The different specular

rays for each different migrated offset collect different traveltime perturbations, so the reflector movements for each offset are computed independently. The points calculated this way describe a "stacking trajectory" that collects the images of reflectors from different constant-offset sections, moves the images to the specified depth point, and stacks the images together. Such a trajectory calculated for any given change in the slowness model is a residual depth migration. Rather than using the calculated residual depth migration, I find the residual time migration that best approximates it using least squares. The least-squares fit combined with the tomography calculation defines the operator that relates changes in interval slowness to changes in the residual slowness. We could form an approximate stacked image after residual depth migration of a fixed depth point by finding the best fitting residual time migration and selecting the appropriate image from the space of all residual time migrations computed with the method of Chapter 2.

3.2.1 Relating changes in interval slowness to changes in migrated position

Δt due to $\Delta w(x,z)$

Consider the reflector shown in Figure 3.1. For a given reflector point and a given dip θ, the family of specular rays, rays that obey Snell's law: angle of incidence = angle of reflection at the reflector point, are the rays along which most reflected energy travels. If the interval-slowness model $w(x,z)$ is perturbed by adding $\Delta w(x,z)$, the traveltime of any ray passing through the perturbation will change. Write the traveltime calculated along a specular ray from source to a subsurface point to receiver as

$$t_{ray} = \int_{ray} w(x,z)\, ds \quad ; \tag{3.1}$$

where s is arc length.

Fermat's principle states that traveltime is stationary with respect to ray path. For small perturbations to the interval-slowness model, $\Delta w(x,z)$, calculate the change in traveltime from a source to a reflector to a receiver with

$$\Delta t = \int_{ray} \Delta w(x,z)\, ds \; . \tag{3.2}$$

Thus, Fermat's principle implies we can find the change in traveltime by integration of

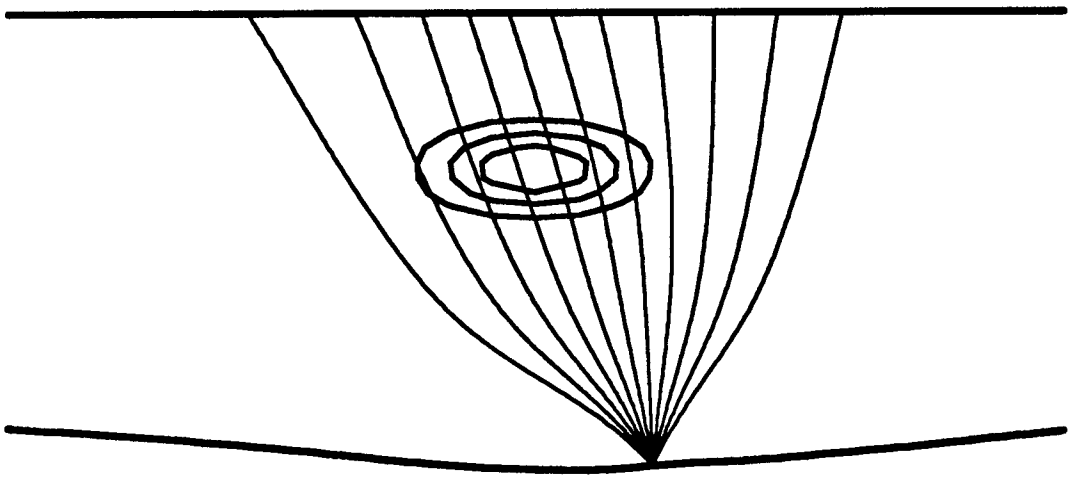

FIG. 3.1. Specular rays for a dipping reflector. If the specular ray for a given offset goes through the slowness anomaly, the position of the reflector will be perturbed.

the anomalous slowness along the unperturbed ray.

$\Delta\sigma_h$ due to Δt

A change in traveltime along a specular ray caused by a change in interval slowness causes reflector images to move. We wish to find the reflector image that moves to a fixed depth point of interest. In effect this requires calculating a residual depth migration. Since the next part of the operator calculation would fit the residual depth migration with a residual time migration, I use this opportunity to make a simplifying approximation. Rather than calculating reflector positions based on residual depth migration which requires extensive ray-tracing or other traveltime computations, I directly convert the change in traveltime to an effective residual time migration for each offset.

$$t = w\left[\sqrt{(x-\xi-h)^2+z^2}+\sqrt{(x-\xi+h)^2+z^2}\right] \ ; \tag{3.3}$$

$$t+\Delta t = w'\left[\sqrt{(x-\xi-h)^2+z^2}+\sqrt{(x-\xi+h)^2+z^2}\right] \ . \tag{3.4}$$

The two equations above state that an accumulated change in traveltime Δt can be interpreted as an effective residual slowness, $\sigma_h = (\Delta t + t)/t$, where t is the original total traveltime along the specular rays from source to depth point to receiver. Equations (3.3)

and (3.4) are just a restatements of equations (2.6) and (2.8) keeping the depth point fixed rather than the traveltime fixed.

Equations (3.3) and (3.4) imply that a change in traveltime is accounted for with reflector movement along a time-migration trajectory in a medium with the average of the slownesses encountered along the original rays. In reality, the traveltime is accounted for with motion along a depth-migration trajectory in the true interval-slowness model. The approximation in equations (3.3) and (3.4) can be improved by computing the traveltime change along the same time-migration trajectory but in the true interval-slowness model.

The preceding discussion assumes that the interval velocity is "smooth" within the range of motion of reflectors to our point of interest. If the assumption is true, residual time migration locally resembles residual depth migration. When the assumption is not true, the mapping between original migrated position and original migrated dip to new migrated position and new migrated dip can change rapidly and will not resemble the constant-velocity derived map. Then, residual depth migration is necessary. However, if residual depth migration is necessary for the individual offsets and cannot be approximated with residual time migration, it is unlikely that fitting the residual migration of each independent offset with the kinematics of one overall residual slowness (done in the next section) will be meaningful; nor is it likely that a coherent event will show up in a stacked section at this location.

3.2.2 Relating changes in migrated position to changes in residual slowness for a fixed depth point

The stacking trajectory computed in the previous section is composed of the independent movements of the different constant-offset sections; an image of a depth point can be formed by stacking over that trajectory. Rather than just stacking with that trajectory, it is more efficient to use the space of all possible residual time migrations to find the stacked image of the point of interest. This requires finding the single residual time migration that best fits the independent residual constant-offset migrations. Recall that residual prestack migration has three parts: residual NMO, residual DMO, and residual zero-offset migration. To fit the computed stacking trajectory we may be required to use different amounts of correction from each part (e.g., a different residual NMO velocity than zero-offset residual-migration velocity). Rather than fitting all three corrections separately, I force the residual-DMO correction to be consistent with the residual-NMO correction and

I only use information from the NMO component and the zero-offset residual-migration component. If residual time migration fits the stacking trajectory perfectly, the residual-NMO and residual-DMO parts are consistent. As long as the interval slowness is smooth, there will only be slight deviations of the fit from the true stacking trajectory, so fitting the residual-NMO part of residual NMO+DMO is all that is necessary.

Δz_h due to $\Delta \sigma_h$

Although the reflector point of interest may have arbitrary dip, interpret the independent residual slownesses, σ_h computed by the previous step, as if the reflector we were trying to image has zero dip. Doing this assumes we have correctly applied residual DMO; since after residual DMO, we can treat all reflectors at a given depth as if they had zero dip. Write the hypothetical zero-dip stacking trajectory as

$$z_h = \sqrt{\sigma_h^2 z_0^2 + (\sigma_h^2 - 1)h^2} \quad . \tag{3.5}$$

Equation (3.5) is just a form of residual NMO plus residual depth conversion. Figure 3.2 shows stacking trajectories made with this equation. As residual slowness σ_h changes, both the curvature and the zero-offset intercept of the stacking trajectory change.

Equation (3.5) converts the problem of finding a best fitting stacking trajectory implied by residual prestack migration to one implied by residual NMO and residual depth conversion. Converting the dipping reflectors to flat reflectors is valid as long as the DMO correction implied by the single residual slowness we get after fitting adequately describes the DMO needed by the individual offsets.

$\Delta \gamma$ and $\Delta \tau$ due to Δz_h

Equation (3.5) is a residual-NMO equation, but it explicitly couples residual zero-offset migration (for zero-dip, residual depth conversion) and residual NMO. When the reflector movement of all offsets is described by one best fitting residual-moveout curve, it is necessary to separate residual NMO and residual zero-offset migration. Rather than having one residual slowness for each offset, we will have only one residual slowness for the NMO correction γ and one position of the reflector after residual zero-offset migration τ. From

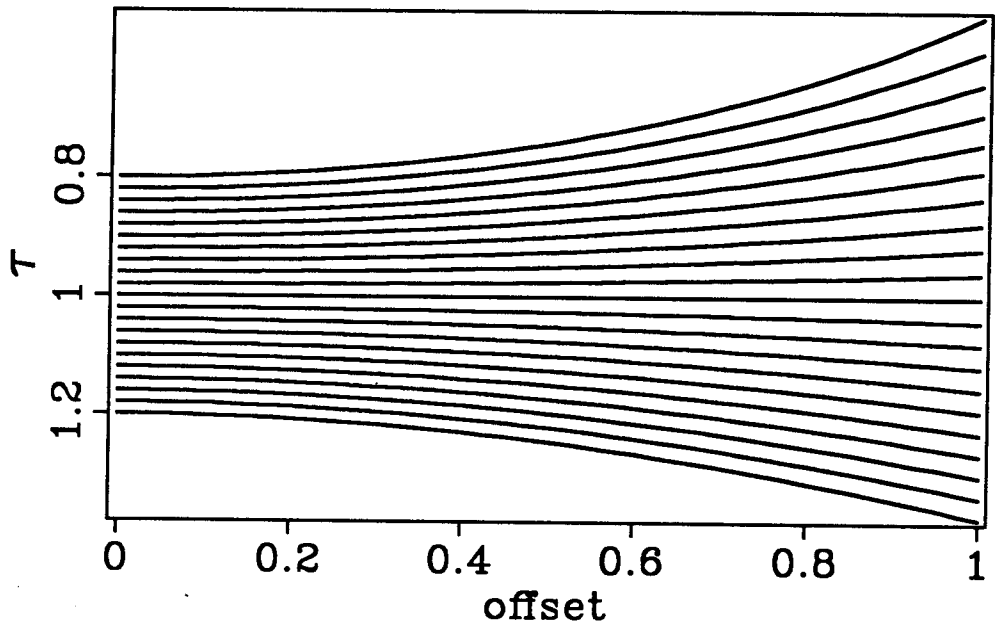

FIG. 3.2. Stacking trajectories for residual NMO with residual zero-offset migration left in.

equation (3.5), substitute $\gamma = \sigma$ and then $\tau = \gamma z_0$ to obtain

$$z_h = \sqrt{\tau^2 + (\gamma^2 - 1)h^2} \ . \tag{3.6}$$

Figure 3.3 shows stacking trajectories for equation (3.6). The zero-offset intercept of each trajectory stays at a fixed τ. Letting τ and γ be independent uncouples the residual NMO from the residual zero-offset migration. If the required residual migration is exactly a time migration, then the information obtained from either τ or γ is the same. When the residual migration is a depth migration, τ and γ contain independent information. Since it is the smallest correction of the three, the residual-DMO correction implied by γ will often be adequate even when the residual-NMO and zero-offset residual-migration components are not consistent with residual time migration (Deregowski, 1990) (also see Figure 2.7).

Now fit the movement of the hypothetical zero-dip reflectors on each constant-offset

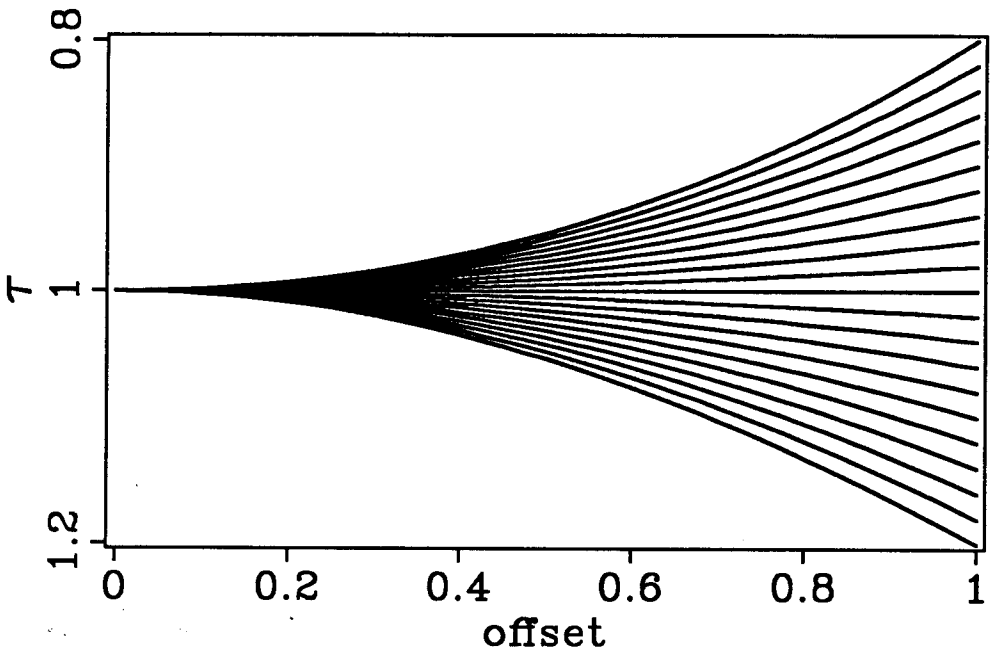

FIG. 3.3. Stacking trajectories for residual NMO alone. These are now stacking trajectories for a fixed event.

section, Δz_h computed in the last sections, with changes in the residual NMO curve computed using equation (3.6). Equation (3.6) is nonlinear in the variables γ and τ; so linearize it about particular values of γ and τ by finding the derivatives of z_h with respect to γ and τ and expressing a small change in z_h as a linear combination of small changes in γ and τ.

$$\Delta z_h = \frac{\partial z_h}{\partial \gamma}\Delta\gamma + \frac{\partial z_h}{\partial \tau}\Delta\tau \quad . \tag{3.7}$$

The expressions for the derivatives $\partial z_h/\partial\gamma$ and $\partial z_h/\partial\tau$ are

$$\frac{\partial z_h}{\partial \gamma} = \gamma h^2/\sqrt{\tau^2 + (\gamma^2 - 1)h^2}\ ; \tag{3.8}$$

$$\frac{\partial z_h}{\partial \tau} = \tau/\sqrt{\tau^2 + (\gamma^2 - 1)h^2}\ . \tag{3.9}$$

Immediately following prestack depth migration before the slowness model is changed, we linearize about the γ and τ that produce no residual moveout, namely $\gamma = 1$ and $\tau = z$.

As the slowness model is perturbed the reference values used for linearization change.

Convert small movements of the different hypothetical zero-dip reflectors Δz_h computed in the last sections to changes in the residual-NMO curve computed using equation (3.7) by minimizing in the least-squares sense

$$E = \sum_{h_{min}}^{h_{max}} (\Delta z_h - \frac{\partial z_h}{\partial \gamma}\Delta\gamma - \frac{\partial z_h}{\partial \tau}\Delta\tau)^2 \quad . \tag{3.10}$$

Write the normal equations that follow as

$$\begin{pmatrix} \sum_{h_{min}}^{h_{max}} (\frac{\partial z_h}{\partial \gamma})^2 & \sum_{h_{min}}^{h_{max}} (\frac{\partial z_h}{\partial \gamma})(\frac{\partial z_h}{\partial \tau}) \\ \sum_{h_{min}}^{h_{max}} (\frac{\partial z_h}{\partial \gamma})(\frac{\partial z_h}{\partial \tau}) & \sum_{h_{min}}^{h_{max}} (\frac{\partial z_h}{\partial \tau})^2 \end{pmatrix} \begin{pmatrix} \Delta\gamma \\ \Delta\tau \end{pmatrix} = \begin{pmatrix} \sum_{h_{min}}^{h_{max}} (\frac{\partial z_h}{\partial \gamma})\Delta z_h \\ \sum_{h_{min}}^{h_{max}} (\frac{\partial z_h}{\partial \tau})\Delta z_h \end{pmatrix} \quad . \tag{3.11}$$

The solution to the least-squares problem of equation (3.11), $\Delta\gamma$ and $\Delta\tau$, gives changes in the residual-moveout curve that best fits the changes in stacking trajectories for a fixed depth point. Symbolically write this solution as the operator $\mathbf{L}$ where

$$\begin{pmatrix} \Delta\gamma \\ \Delta\tau \end{pmatrix} = \begin{pmatrix} \mathbf{L}_\gamma \\ \mathbf{L}_\tau \end{pmatrix} \Delta z_h \quad . \tag{3.12}$$

Figures 3.4 and 3.5 show the impulse response of the operators $\mathbf{L}_\gamma$ and $\mathbf{L}_\tau$. The value of the operator as a function of offset is the change in γ or τ due to a unit change Δz_h in the stacking trajectory at that offset. Figures 3.6 and 3.7 show examples of best fitting residual-moveout curves for perturbations to stacking trajectories at small and large offsets. The effect of a perturbation to the stacking trajectory at small offsets is opposite to the effect of a perturbation at large offsets. A positive perturbation to the stacking trajectory at inner offsets leads to a negative change in the apparent residual slowness γ and leads to a pull-down of the zero-offset of the best fitting residual-moveout curve. A positive perturbation to the stacking trajectory at outer offsets leads to a positive change in the apparent residual slowness γ and leads to a pull-up of the zero-offset of the best fitting residual-moveout curve.

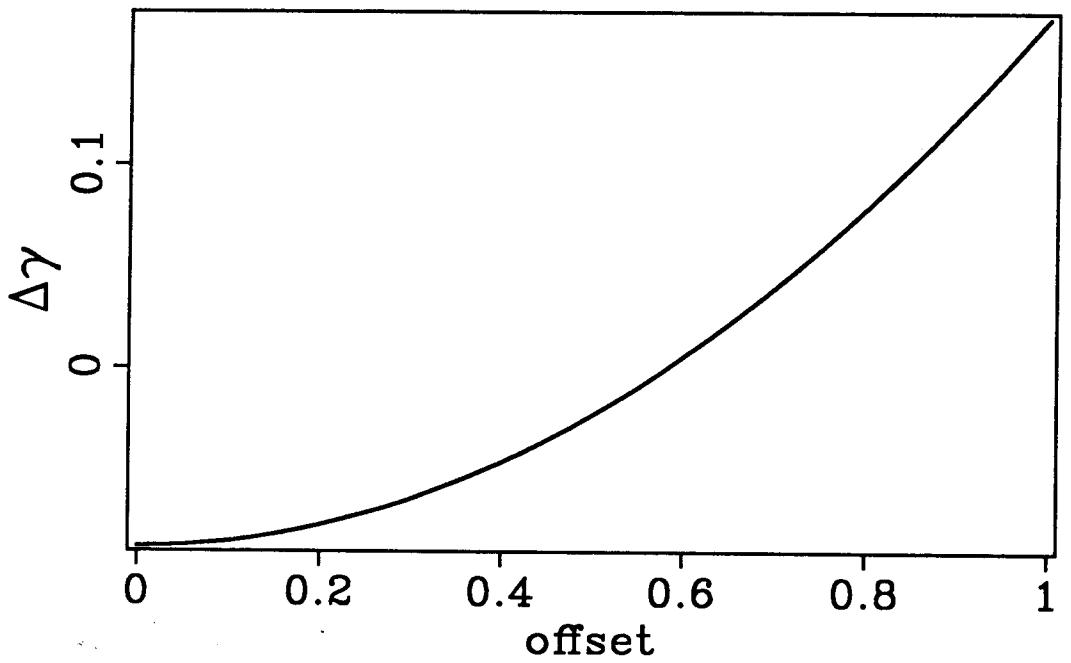

FIG. 3.4. Impulse response of $\mathbf{L}_\gamma$. The value at a given offset is the change in γ caused by a unit change in the z_h for that offset.

3.2.3 Building the filtered traveltime-tomography operator G

Equation (3.12) can be combined with the tomography and other calculations to write one operator that relates changes in interval slowness to changes in the parameters that describe the best fitting residual migration at a given point in space. $\partial t/\partial w$ converts changes in interval slowness to changes in traveltime; it is the tomography operator. $\partial \sigma_h/\partial t$ converts changes in traveltime to changes in the residual time-migrated position for the different offsets. $\partial z_h/\partial \sigma_h$ converts the residual time migrations of each offset into equivalent zero-dip reflector movement. Finally, the least-squares fit converts Δz_h to changes in the parameters of the residual-moveout curve. Writing the operator in compact notation,

$$\begin{pmatrix} \Delta\gamma \\ \Delta\tau \end{pmatrix} = \begin{pmatrix} \mathbf{L}_\gamma \\ \mathbf{L}_\tau \end{pmatrix} \frac{\partial z_h}{\partial \sigma_h}\frac{\partial \sigma_h}{\partial t}\frac{\partial t}{\partial w}\Delta w = \begin{pmatrix} \mathbf{G}_\gamma \\ \mathbf{G}_\tau \end{pmatrix} \Delta w \ . \tag{3.13}$$

The linear operator $\mathbf{G}$ in equation (3.13) relates changes in the interval-slowness model to changes in the best fitting residual-moveout curve at a fixed spatial location.

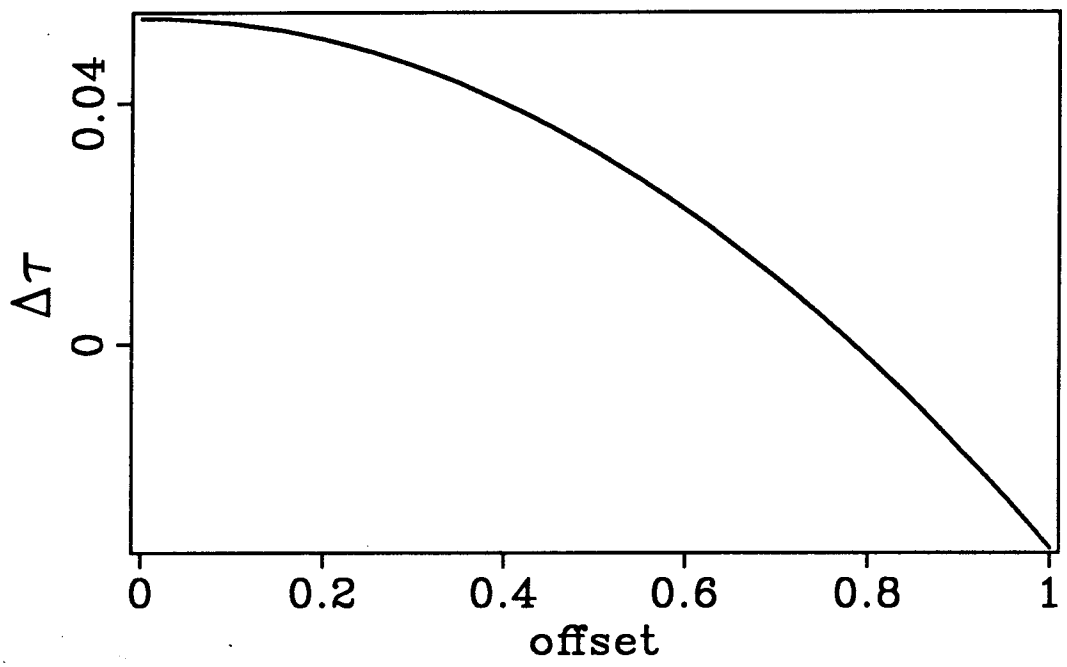

FIG. 3.5. Impulse response of $\mathbf{L}_\tau$. The value at a given offset is the change in τ caused by a unit change in the z_h for that offset.

Analyzing G

The best way to understand the operator **G** is to examine the effect of a local perturbation to the interval-slowness model on a set of reflectors, and to examine the effect of perturbations to the interval-slowness model as a whole on a single reflector point. These correspond to examining a column or a row of the matrix **G** respectively. Plotting the operator responses in (x, z) as we would plot the velocity model or the migrated image helps to visualize the operator. Figure 3.8 shows a row of the **G** operator; the value plotted (denoted by gray-scale intensity) is the effect of a unit perturbation in interval slowness at that point on a single depth point on a horizontal reflector. The single reflector point is at the end of the narrow part of the operator "cone." The top plot gives the effect on γ and the bottom plot gives the effect on τ. Figure 3.9 shows a row of the **G** operator for a dipping reflector. Now the operator cone is tilted, because the specular rays that illuminate the depth point open out from the zero-offset ray that is normal to the reflector. The gray background in all plots indicates no effect; a slowness anomaly here is not intersected by a specular ray and does not change the residual slowness or position of the one event

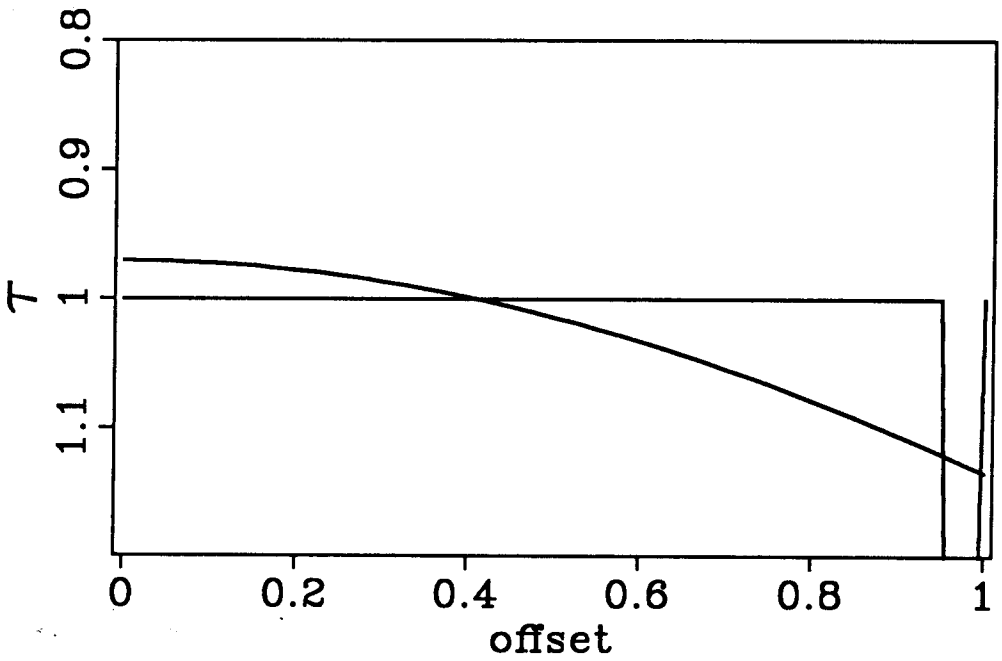

FIG. 3.6. Best fitting stacking trajectory for a change in z_h at an outer offset.

of interest. Lighter shades indicate a positive effect; a positive slowness anomaly in a light area increases γ or τ. Darker shades indicate a negative effect; a positive slowness anomaly decreases γ or τ. Figure 3.10 shows a column of the operator $\mathbf{G}$. The values plotted are the effects in γ and τ of a perturbation to the interval-slowness model on a depth point at that location. In this figure all reflector points have zero-dip. The perturbation in interval slowness is at the top of the operator cone. Figure 3.11 shows a column of operator $\mathbf{G}$ when the reflectors are all dipping with the same 30 degree dip; again the slowness perturbation is at the top of the cone. Now the gray background represents reflector points that do not feel the presence of the anomaly; no specular ray that illuminates these reflector points goes through the anomaly and is recorded by a 2 km long cable. Lightly shaded areas denote reflector points that have a positive correlation between the sign of $\Delta\omega$ and $\Delta\gamma$ or $\Delta\tau$; dark shades denote reflector points that have negative correlation. The further the shade is from the gray background, the stronger the effect.

The lateral-wavenumber spectrum of the operators $\mathbf{G}_\gamma$ and $\mathbf{G}_\tau$ describe how slowness anomalies with different wavelengths cause different changes in the curvature and output position of the residual-migration operator used to make the stacked image of migrated

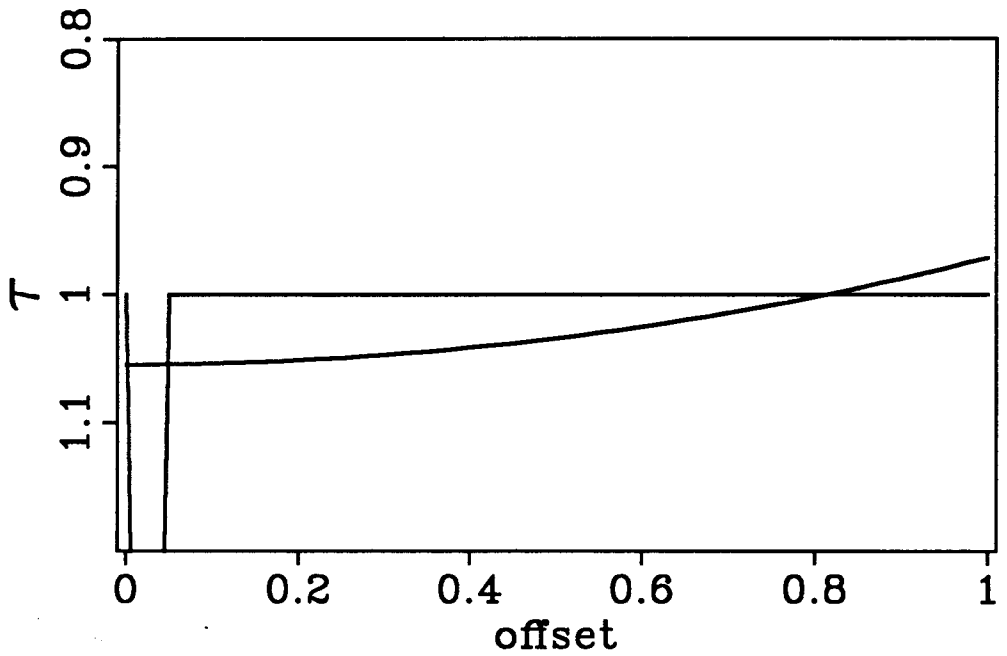

FIG. 3.7. Best fitting stacking trajectory for a change in z_h at an inner offset.

events. Figure 3.12 shows the spectrum of $\mathbf{G}_\gamma$ computed for a point on a flat reflector, a 2 km cable, and for slowness anomalies near the surface of the model. The DC component (wavenumber= 0) shows the change in γ for a laterally constant change to the interval-slowness model near the surface. The greatest response of the operator spectrum occurs at a wavenumber (wavenumber = .45) approximately equal to the distance across the ray fan at the anomaly depth (called the effective cable length). The spectrum has a zero and small values near DC. Slowness anomalies at these combinations of reflector depth, cable length, and anomaly depth cause little or no change to γ of the best fitting residual-moveout curve because the change in the curvature of the residual-moveout curve caused by the inner offsets is canceled by the change caused by the outer offsets. Figure 3.13 shows the spectrum of $\mathbf{G}_\tau$ for the same 2 km cable and for slowness anomalies near the surface. Long-wavelength anomalies that do not affect γ are effective at creating pull-up or push-down. Where there is a zero of the spectrum, a slowness anomaly with that wavenumber has no effect on time-to-depth conversion. The different spectra of $\mathbf{G}_\gamma$ and $\mathbf{G}_\tau$ reinforce the qualitative feeling that the velocity information contained in moveout is different from the velocity information contained in reflector positioning.

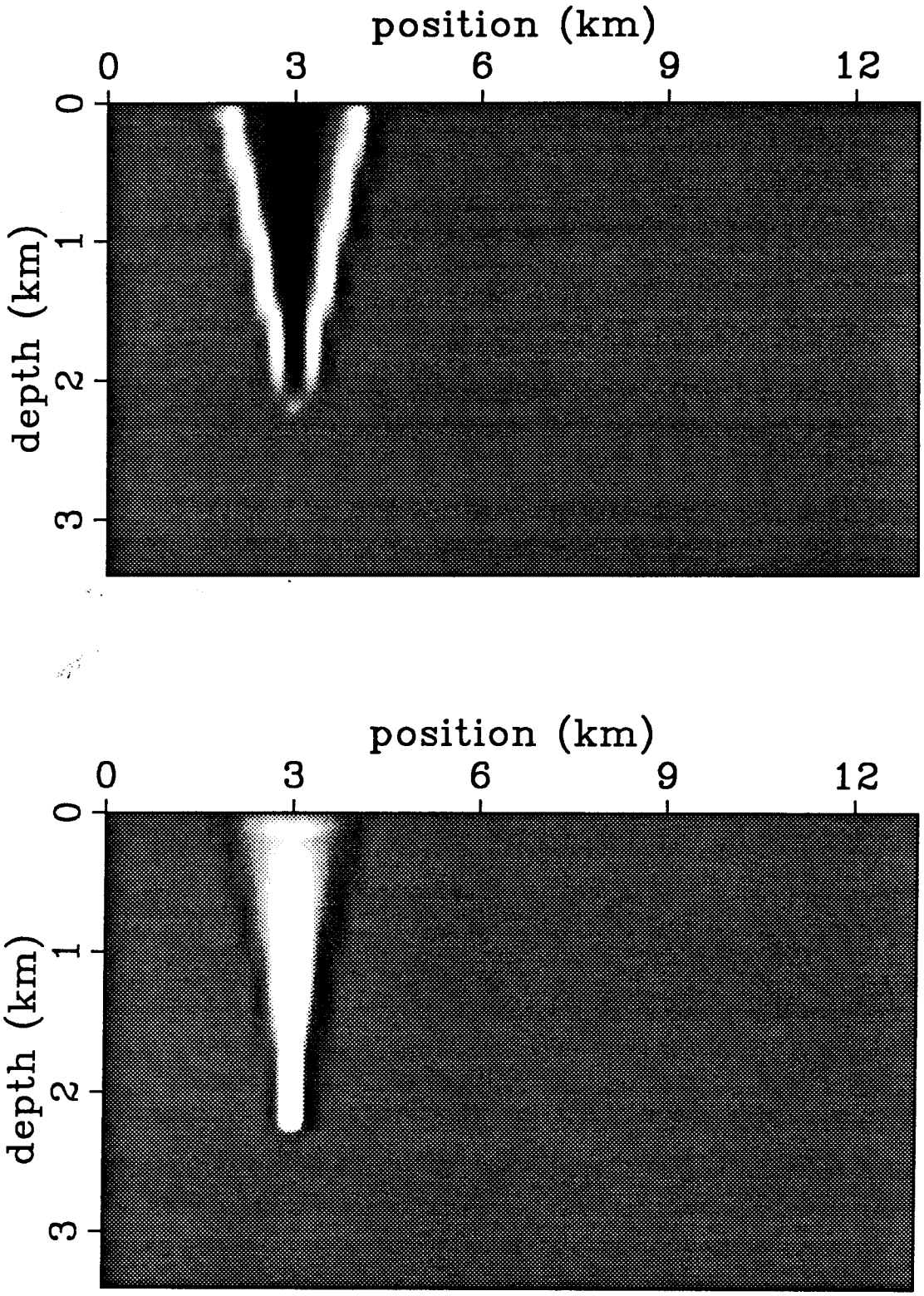

FIG. 3.8. A row of the operator **G** for a point on a horizontal reflector. The reflector point is at the bottom of the operator cone.

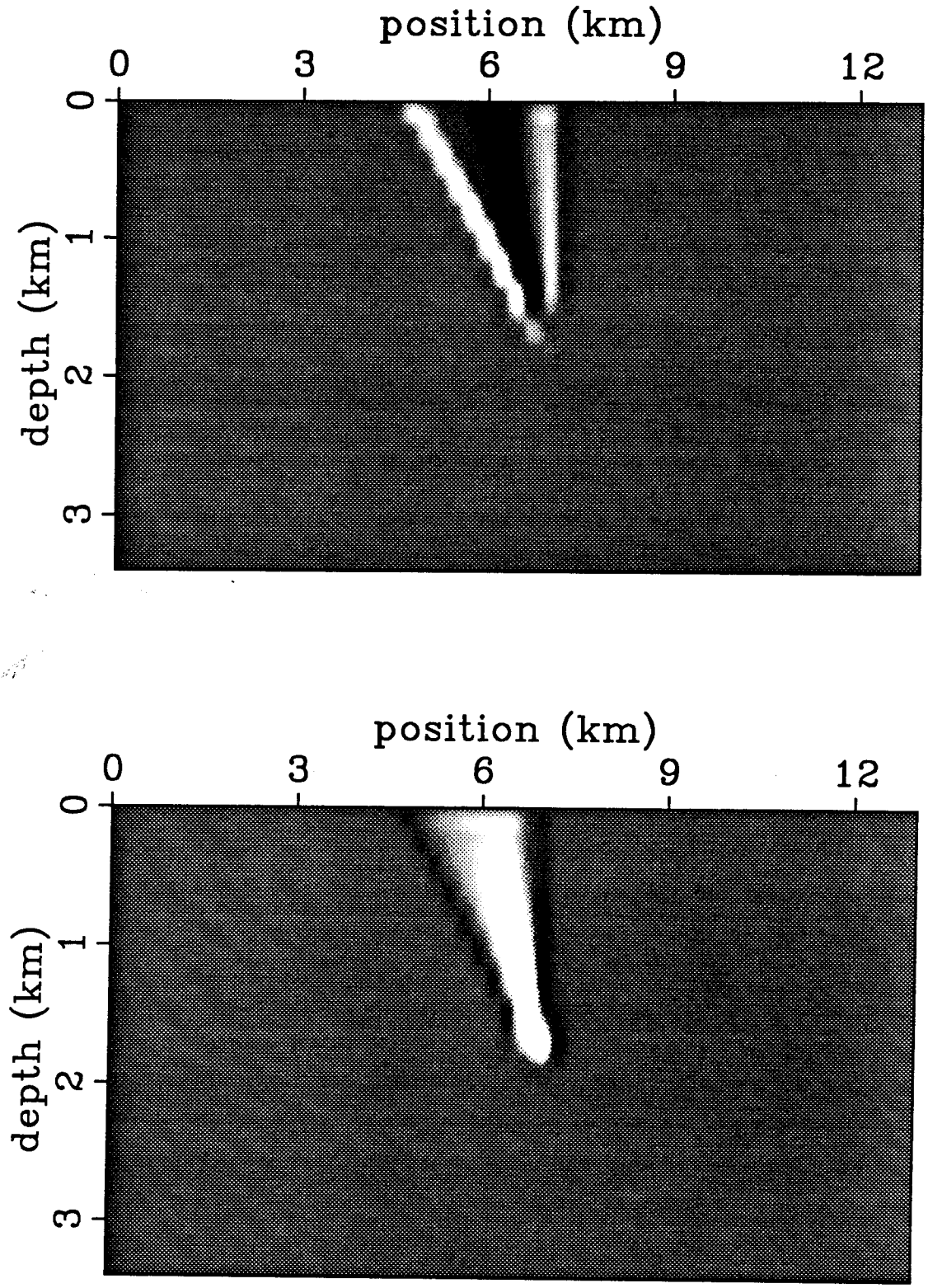

FIG. 3.9. A row of the operator **G** for a point on a dipping reflector. The reflector point is at the bottom of the operator cone.

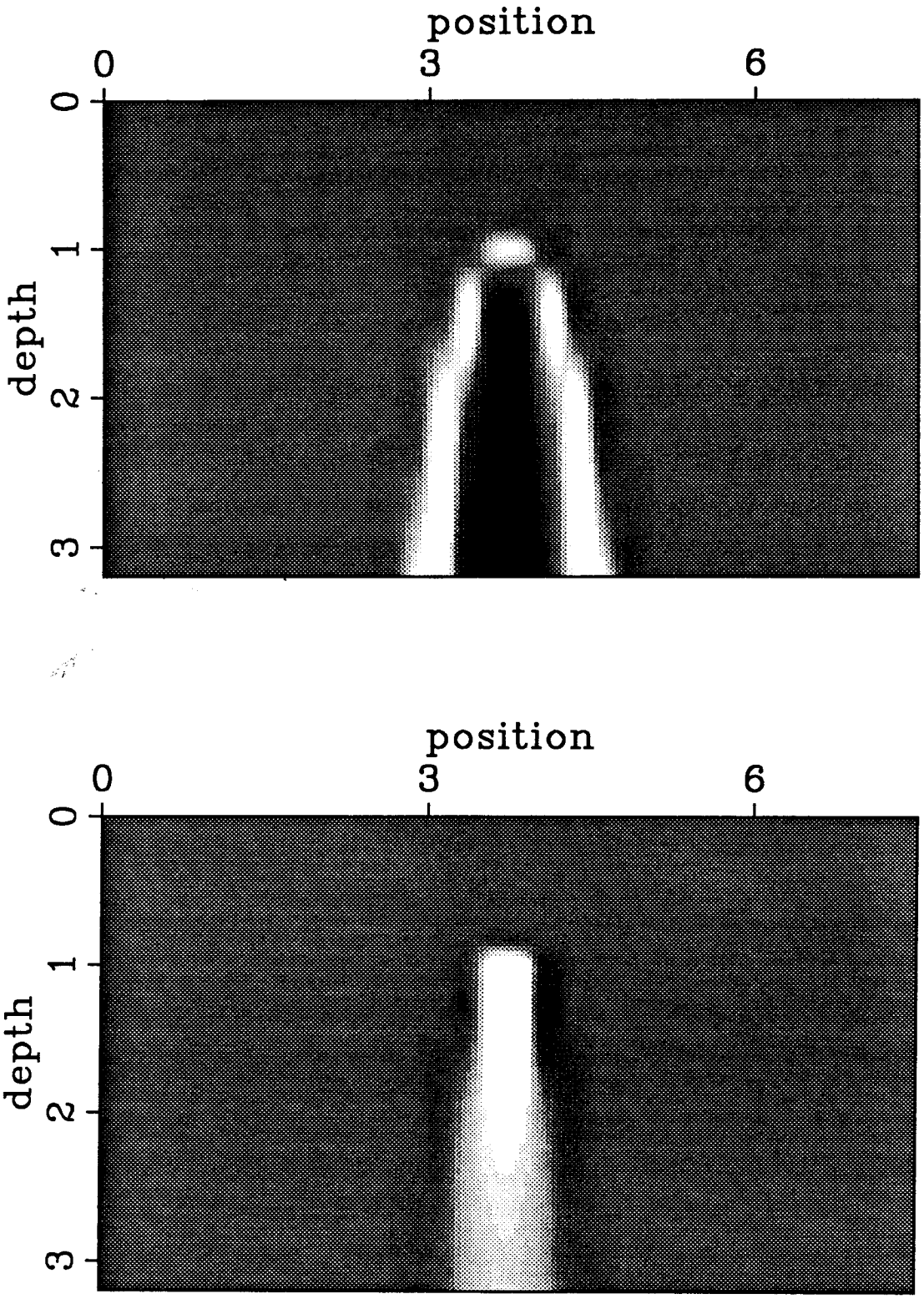

FIG. 3.10. A column of the operator **G**. All reflector points are on horizontal reflectors. The slowness anomaly is at the top of the cone.

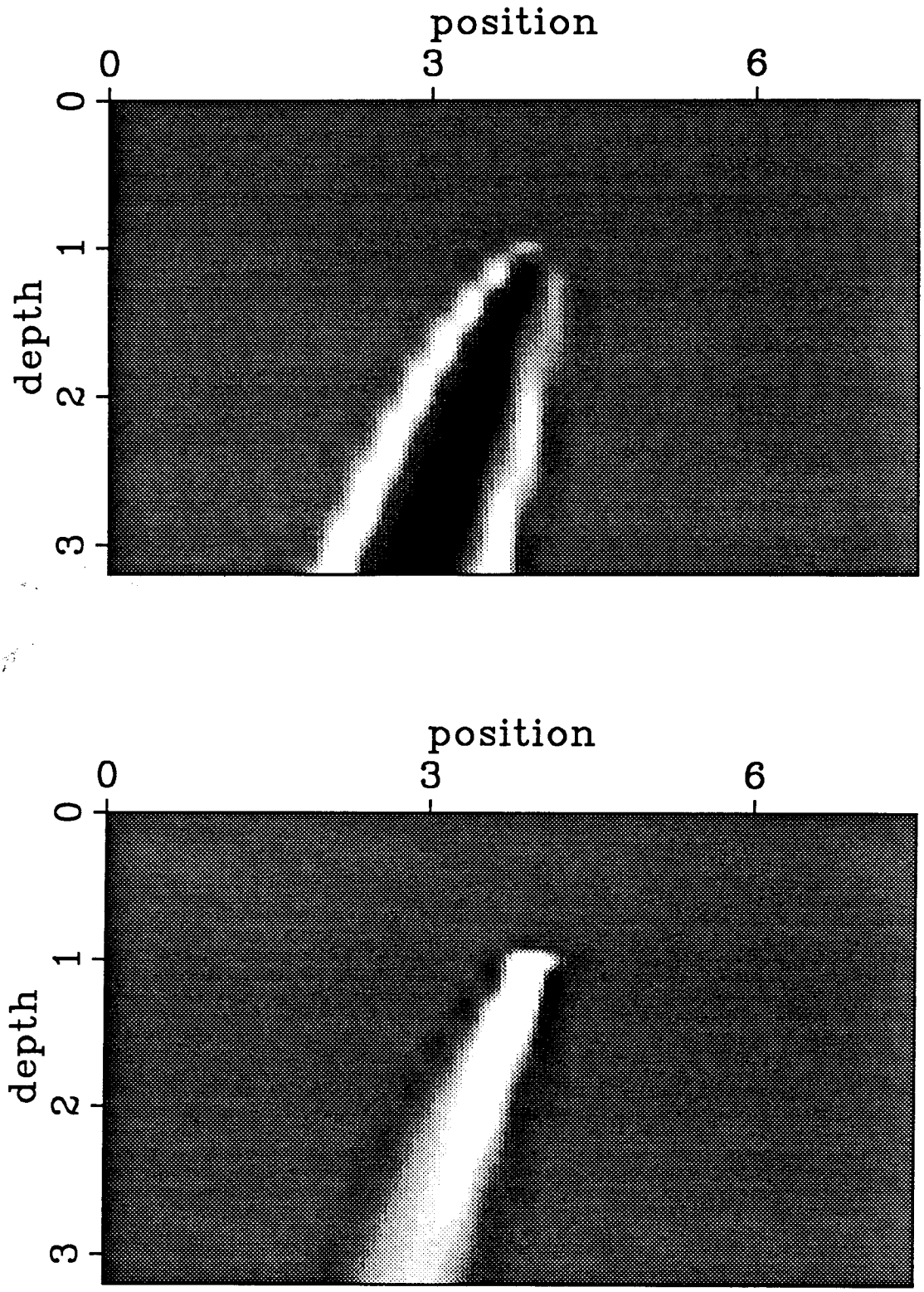

FIG. 3.11. A column of the operator **G**. All reflector points are on 30 degree dipping reflectors. The slowness anomaly is at the top of the cone.

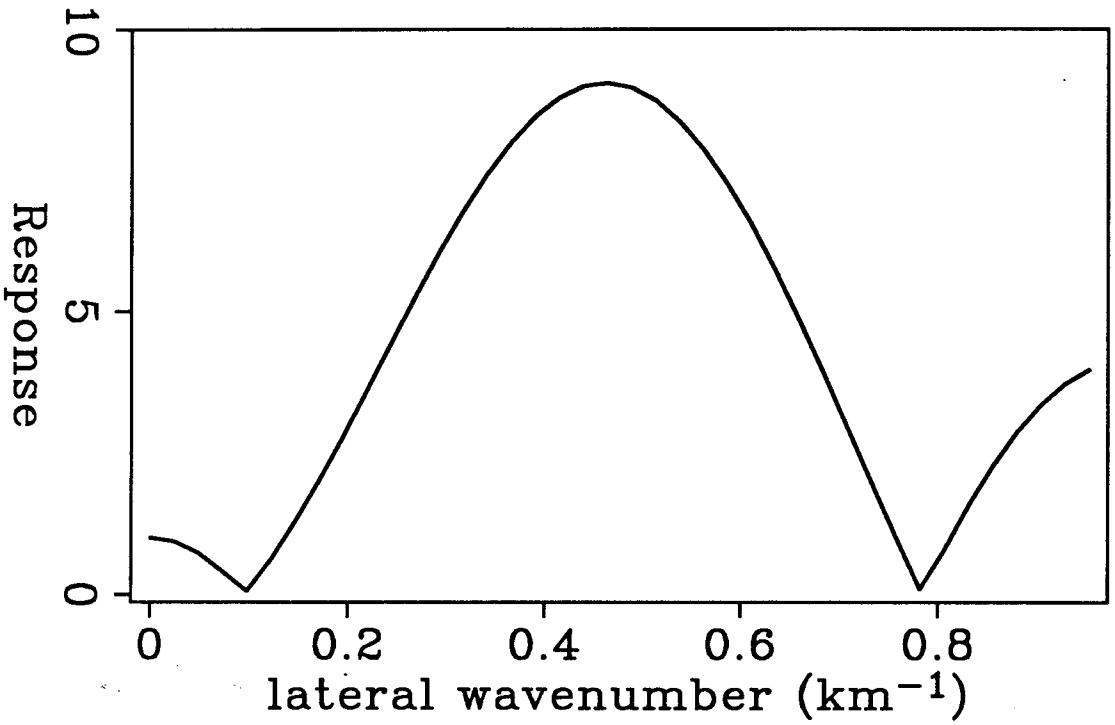

FIG. 3.12. Amplitude spectrum of G_γ vs. lateral wavenumber for shallow slowness anomalies. The greatest response occurs for wavenumbers approximately the same as the cable length. DC and long-wavelength anomalies affect the residual moveout only slightly.

3.3 Reflector tomography for a fixed event

The interval-slowness model and the linear operator just described are evaluated at fixed spatial locations. However, we need to find an operator that relates changes in interval slowness to changes in the residual slowness for fixed events. Since the images of events move as the interval slowness changes, the event that is displayed at a fixed depth point changes as interval slowness changes.

Denote true spatial locations with coordinate pairs (x, z). The traveltime-tomography calculations are carried out in this domain; the interval-slowness model is specified in this domain, and the true migrated positions of events are specified in (x, z). The positions of events after the initial prestack depth migration will be denoted by (ξ, η). When we perform residual NMO+DMO for a range of residual slownesses, the image of any given event stays fixed in (ξ, η); because residual NMO+DMO omits the repositioning of reflectors controlled by residual zero-offset migration. Implicitly, the residual-slowness

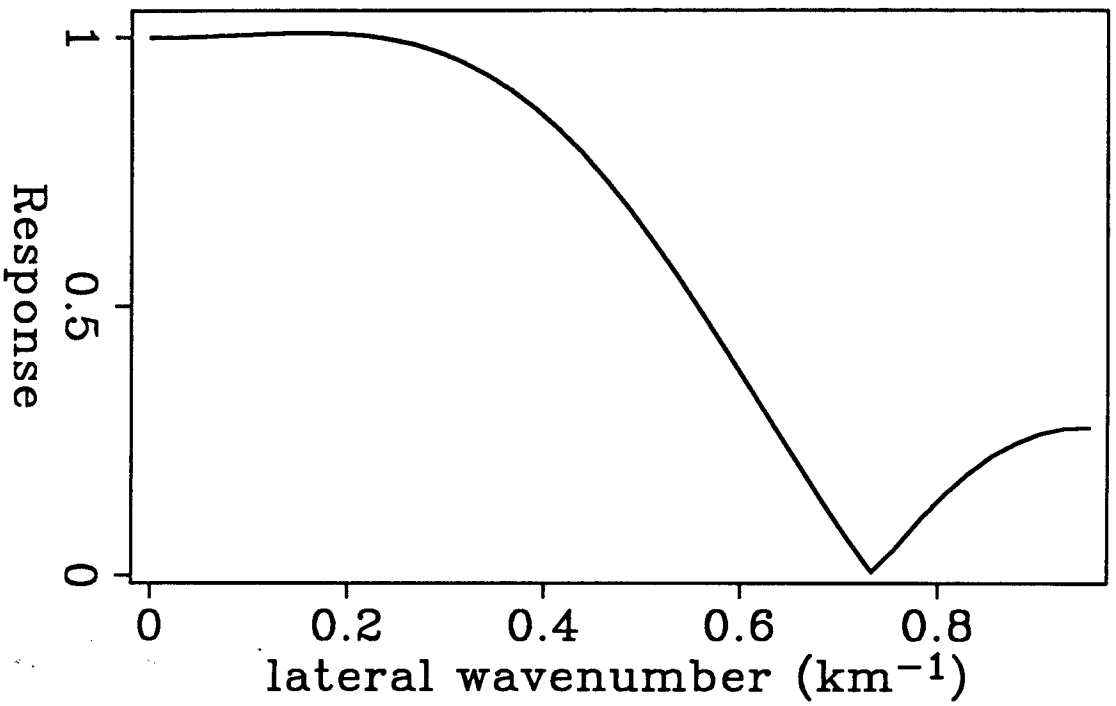

FIG. 3.13. Amplitude spectrum of $\mathbf{G}_\tau$ vs. lateral wavenumber for shallow slowness anomalies. The greatest response occurs for wavenumbers near DC, these anomalies are effective in creating pull-up or push-down. Shorter-wavelength anomalies cause less pull-up or push-down.

value tells the time-migrated position of reflector since we could apply residual zero-offset migration after residual NMO+DMO.

Initially, just after prestack depth migration and before the interval-slowness model changes, the (ξ, η) location of a given event is also its (x, z) location. Somewhat confusingly, both of these domains are "depth" domains; however, the (ξ, η) coordinates only give the correct location of the image when there is no change to the interval-slowness model. As the interval slowness changes, the (ξ, η) coordinates of an event need zero-offset residual event migration to convert them to (x, z).

3.3.1 Nonlinear forward modeling with G

G, the operator for a fixed depth point, is a linear operator; changes in γ and τ are linearly related to changes in the interval-slowness model. We want the operator that relates changes in interval slowness to changes in residual slowness for fixed events. To

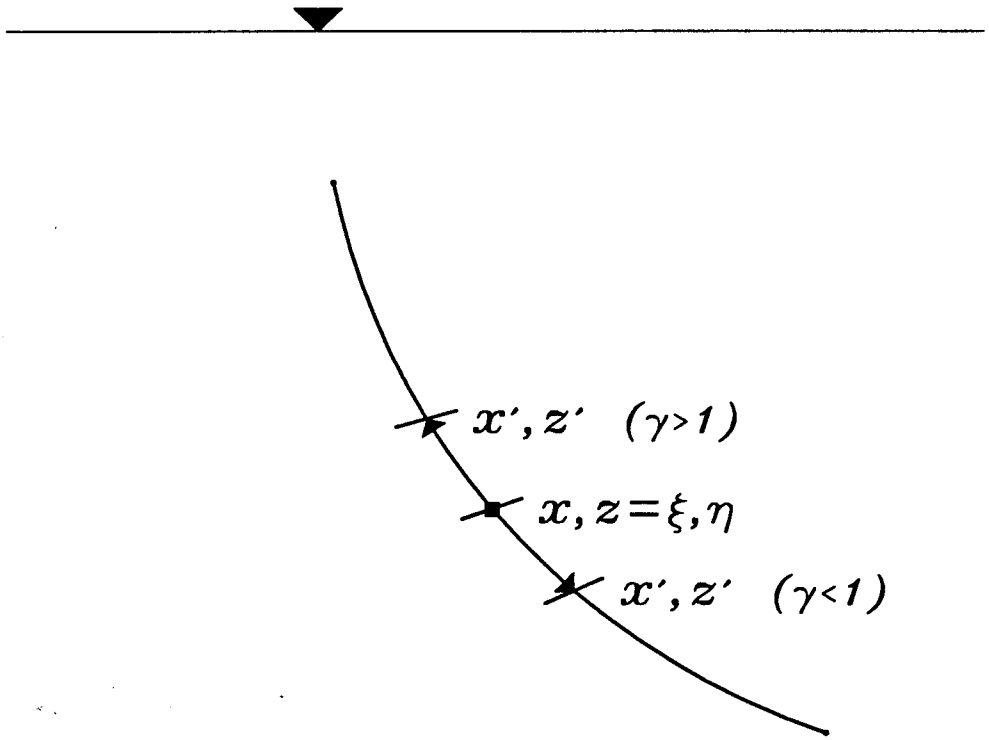

FIG. 3.14. Possible locations of an event (ξ, η) initially at (x, z) after different amounts of residual time migration. The residual time-migrated locations approximate the location of the event after residual depth migration.

follow movement of events, or the change in where a fixed event is displayed in depth, the operator will become nonlinear.

Since I use the reflector positions implied by residual time migration, all possible locations of a single event (defined by a single location and migrated dip) lie along a curvilinear path in (x, z) rather than at arbitrary spatial locations, which would be the case if I used residual depth migration. This time-migration path, shown in Figure 3.14, gives the possible locations of a single reflector with a given dip for all possible residual time-migration slownesses. This curve describes movement in true depth (x, z). Conversely, Figure 3.15 shows all possible event locations that a fixed depth point and dip maps to for various residual slownesses. This curve describes the apparent movement of a fixed depth point in pseudo-depth (ξ, η). These two curves describe a mapping and its inverse from event space to depth space and vice-versa. The middle reflector on Figures 3.14 and 3.15 at $(\xi, \eta) = (x, z)$ shows the initial state of the mapping just after prestack depth migration.

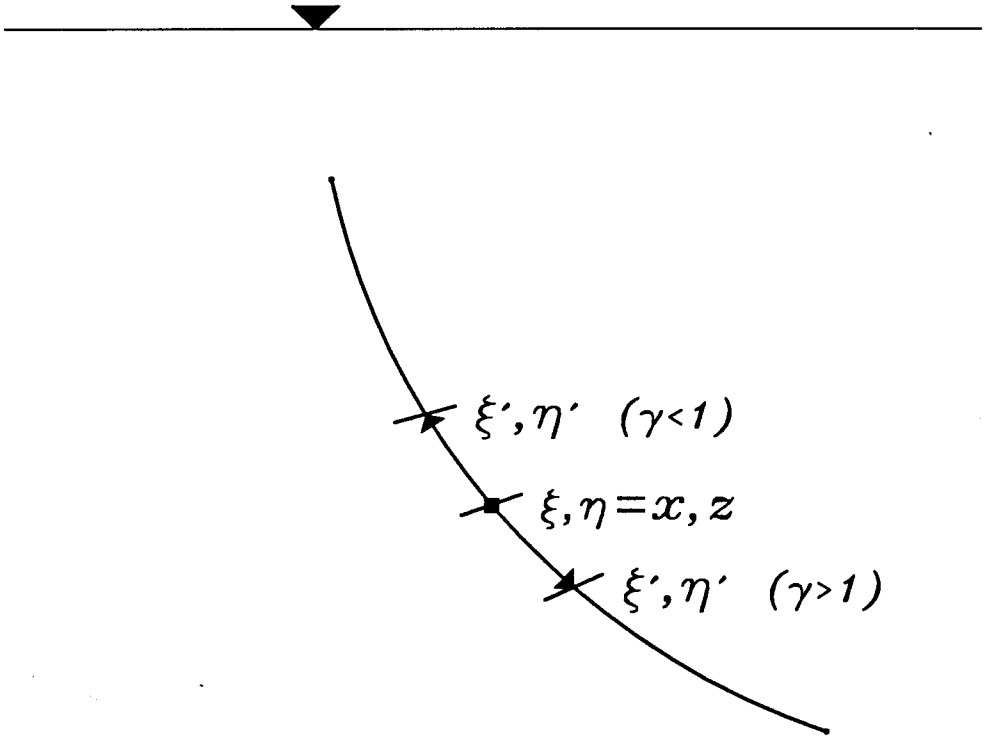

FIG. 3.15. A change in interval slowness causes the event that maps to a fixed (x, z) to change. Range of possible events (ξ', η') that can migrate to a fixed (x, z). Initially this (x, z) maps to (ξ, η).

Making a change in the interval-slowness model and applying **G** changes $\gamma(x, z)$ and alters the mapping from (x, z) to (ξ, η). As shown in Figure 3.16, to find γ for a fixed (ξ, η), find the new true-depth coordinates (x', z') that map to the event of interest and find its updated value of γ. In practice, apply **G** to find $\Delta\gamma$ the change in curvature, and $\Delta\tau$, the change in the zero-offset intercept of the stacking trajectory for several positions along the curve of possible locations for each event. Then find the spatial location that now displays the fixed event of interest (ξ, η) by inverse interpolation. The updated γ for this location is the γ for the event of interest and can be found by interpolation of the updated γ's along the curve of reflector positions.

3.3.2 Linear forward modeling with G

There are several reasons why it is worthwhile to linearize the process of finding γ for fixed events described in the previous section. First, a linear operator can be precomputed and stored; thus, it can be used for many different Δw without recalculation. Second, the

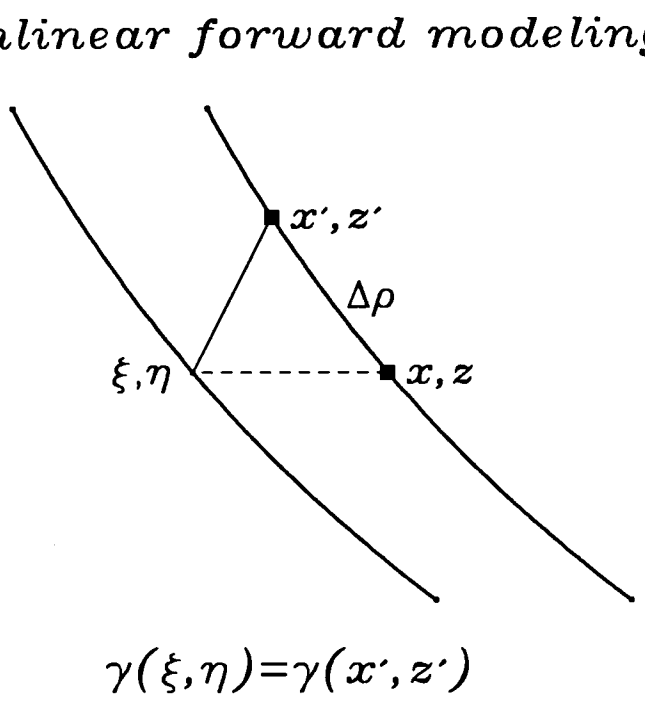

FIG. 3.16. Mapping between a range of fixed depth points on the right, and fixed events on the left.

behavior of a linear operator is easier to analyze than a nonlinear one. In the next chapter we will use the operator of this chapter to estimate changes to the interval-slowness model using the residual slowness measured from migrated data. To get interval slowness from residual slowness we have to invert the relation between interval slowness and residual slowness. The linearized forward operator and its adjoint or transpose are needed by the iterative inversion algorithm presented in the next chapter.

Recall that the operator $\mathbf{G}$ evaluated for a fixed depth point is linear, and that only the movement of images causes the operator to be nonlinear. Therefore, $\mathbf{G}_\gamma$ can be relabeled as $\partial\gamma(x,z)/\partial w$ and $\mathbf{G}_\tau$ can be relabeled as $\partial\tau(x,z)/\partial w$. This relabeling makes sense when we write Taylor series for γ and τ as a function of the slowness model w as in equations (3.14) and (3.15).

$$\gamma(x,z;w) = \gamma(x,z;w_o) + \int_{\text{model}} \frac{\partial\gamma(x,z;w)}{\partial w}\Delta w\; dx\; dz \quad . \tag{3.14}$$

$$\tau(x,z;w) = \tau(x,z;w_o) + \int_{\text{model}} \frac{\partial\tau(x,z;w)}{\partial w}\Delta w\; dx\; dz \quad . \tag{3.15}$$

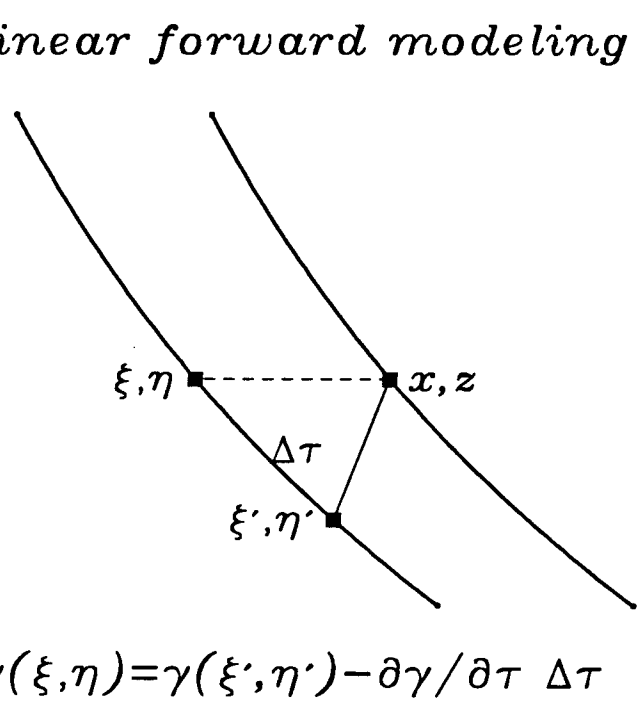

FIG. 3.17. For small perturbations to the interval-slowness model, $\gamma(\xi,\eta)$ can be calculated to first order from $\gamma(\xi',\eta')$, the change in event location $\Delta\tau$ and $\delta\gamma/\delta\tau$. .

The above equations calculate the change in the parameters describing the stacking trajectory for a fixed depth point. As before, we want the parameters of a stacking trajectory for a fixed event. Since the family of events that can map to a fixed depth point and dip lie along a one-dimensional trajectory in (ξ,η), I use τ to measure position along that one-dimensional trajectory. Parameterize the positions of different events that originate at (x,z) with $\xi=\xi(\tau)$ and $\eta=\eta(\tau)$. Through equation (3.15), τ is a function of the interval-slowness model, so write the curvature γ in terms of event locations rather than fixed depth location and as a function of the interval-slowness model.

$$\gamma(\tau;w)=\gamma(\tau_o;w_o)+\int_{\text{model}}\frac{\partial\gamma}{\partial w}\Delta w\,dx\,dz \quad ; \tag{3.16}$$

where $\tau_o=\tau(w_o)$, $\tau=\tau(w)$, and $\tau(w)$ is calculated using equation (3.15). Equation (3.16) is the same as equation (3.14), only the latter expresses γ as a function of event location rather than spatial location. Equation (3.16) gives γ for the new slowness model w but at a new event τ, rather than at the original event τ_o as desired. As shown in Figure 3.17,

to first order, write γ for the new slowness model w for the event at τ_o as

$$\gamma(\tau_o; w) = \gamma(\tau - \Delta\tau; w) = \gamma(\tau; w) - \frac{\delta\gamma}{\delta\tau}\Delta\tau \quad . \tag{3.17}$$

The $\Delta\tau$ in equation (3.17) is the one implied by equation (3.15). $\delta\gamma/\delta\tau$ must be determined from the previous γ's of events along the residual-migration trajectory. In practice, find $\delta\gamma/\delta\tau$ by finite-differencing γ at nearby event locations along the trajectory of event motion. Now combining equations (3.15) and (3.17), solve for the change in γ at a fixed event at τ_o for the change in the slowness model Δw .

$$\gamma(\tau_o; w) = \gamma(\tau_o; w_o) + \int_{\text{model}} \frac{\partial\gamma}{\partial w} - \frac{\delta\gamma}{\delta\tau}\frac{\partial\tau}{\partial w}\Delta w \; dx \; dz \quad . \tag{3.18}$$

Finally, reexpressing the derivatives above as the operators of equation (3.13) write

$$\Delta\gamma(\tau_o) = \left[\mathbf{G}_\gamma - \frac{\delta\gamma}{\delta\tau}\mathbf{G}_\tau\right]\Delta w \quad . \tag{3.19}$$

3.4 Forward modeling example

The operator $\mathbf{G}$ can be used to predict the effect of a change in interval slowness on the residual slowness of reflectors measured by the method of Chapter 2. Figure 3.18 shows an interval-slowness model used to generate synthetic data with finite-difference acoustic modeling. Dark areas are high velocity and light areas are low velocity. To test the operator, I migrated the constant-offset sections with an incorrect slowness model, a constant slowness equal to the slowness above the first reflector away from any perturbations. Figure 3.19 shows the migrated and stacked section. The effect of using the incorrect slowness model is apparent; there is a long-wavelength pull-up on the lower reflector and a short-wavelength push-down on both reflectors.

I applied residual NMO+DMO for a range of residual slownesses to the unstacked migrated constant-offset sections and formed a residual-slowness semblance cube. Figure 3.20 shows horizon residual-slowness analyses for the two reflectors obtained by slicing through the semblance cube along the reflector positions. The obvious "W" patterns of the peaks of stack semblance are caused by the small anomaly. The lower reflector also shows a long-wavelength trend in residual slowness. I calculated the operator $\mathbf{G}$ to relate changes

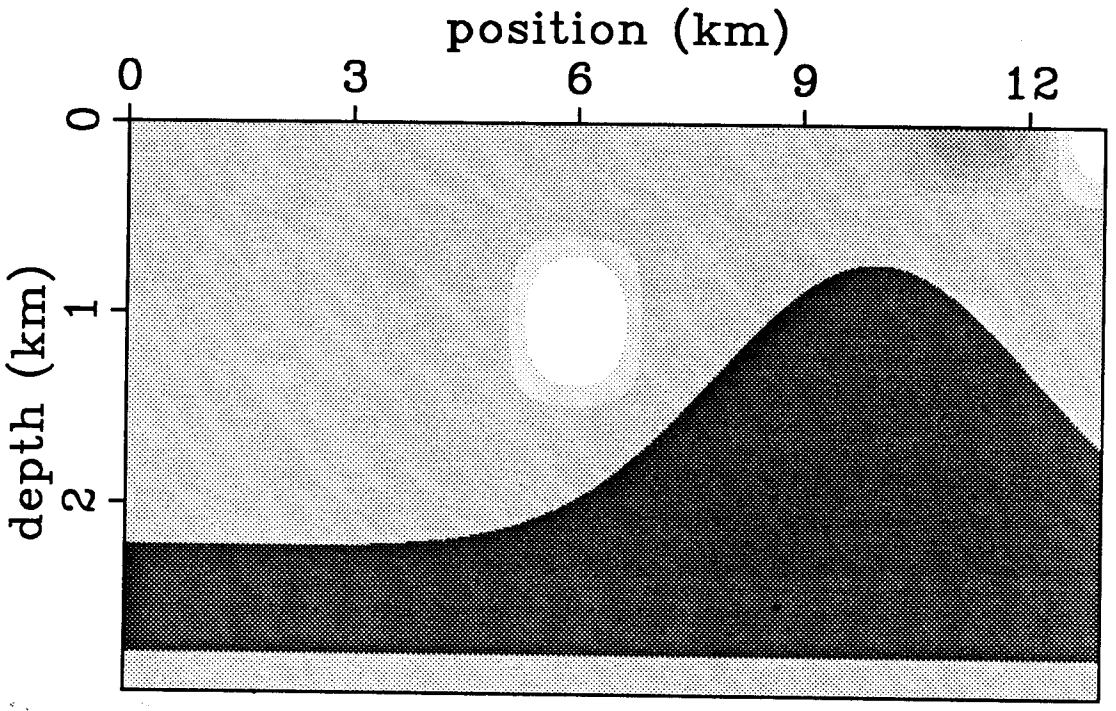

FIG. 3.18. Slowness model used to generate a synthetic data set with finite differences.

in interval slowness and changes in residual slowness for the two events in the image. Applying **G** to the difference between the true slowness model and the slowness model used for migration, the dark lines in Figure 3.20 show the predicted residual slowness γ. The effect of the shallow "blob" anomaly on the upper reflector is predicted accurately. The long-wavelength trend of the semblance peaks of the lower reflector is also predicted accurately. The predicted γ's do not lie on the peaks of the semblance where the lower reflector is affected by the shallow anomaly; the predicted effect of the anomaly is less than the observed effect.

There are two factors that contribute to the inaccurate prediction. First, the lower reflector is grossly mispositioned. If residual time migration does not predict all the reflector movement caused by the anomalous slowness, the events will not feel the anomaly the way the operator predicts. The error in the predicted residual positioning is partially caused by using residual time migration instead of residual depth migration in the operator calculation. Second, the changes in traveltime calculated by the operator do not incorporate the effects of ray-bending caused by the anomalous slowness because the operator used

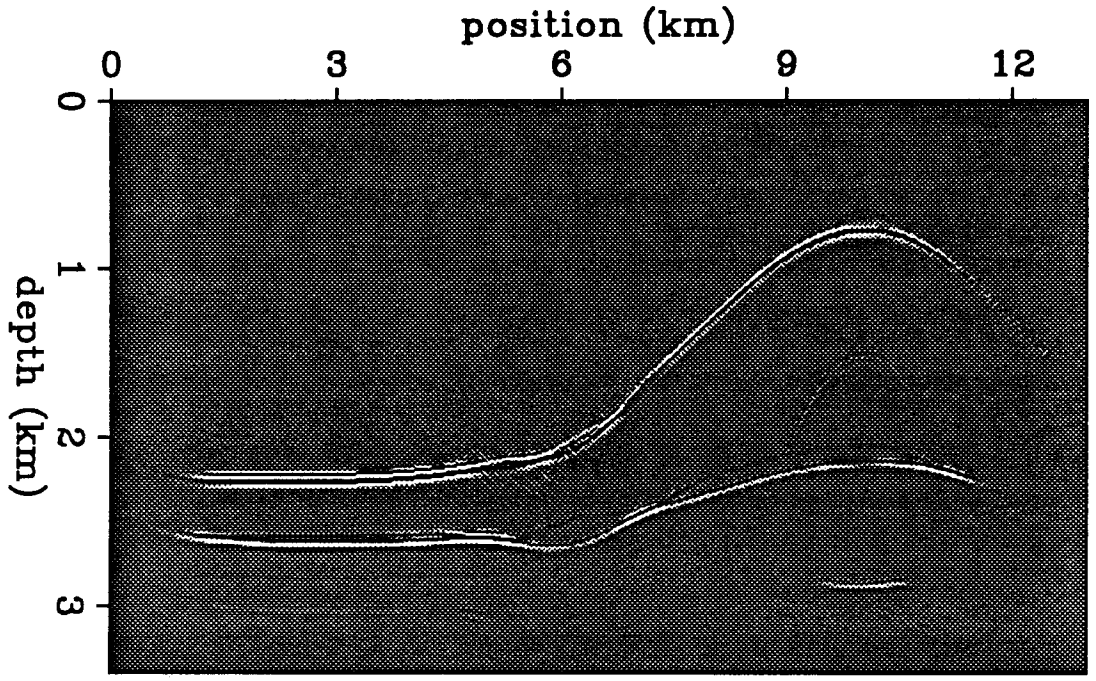

FIG. 3.19. Migrated and stacked section obtained with the incorrect slowness model.

Fermat's principle. The ray-bending not only changes the amount of traveltime perturbation for each given offset, but also rearranges the shape of the operator as it passes over the anomaly. Both of these effects cause nonlinear interaction of the high-slowness local anomaly and the low-slowness anomaly below the first reflector; as a result, **G** does not predict γ accurately where the effects combine.

The approximations made in the construction of **G** affect the estimation of large changes to the interval-slowness model. The results indicate that long-wavelength anomalies should be estimated and removed before estimating short-wavelength anomalies. Then, after the reflector positions are nearly correct and the longest-wavelength components of the interval-slowness model are known, the effects of short-wavelength anomalies will be more accurately predicted by **G**, e.g., for the top reflector in Figures 3.19 and 3.20.

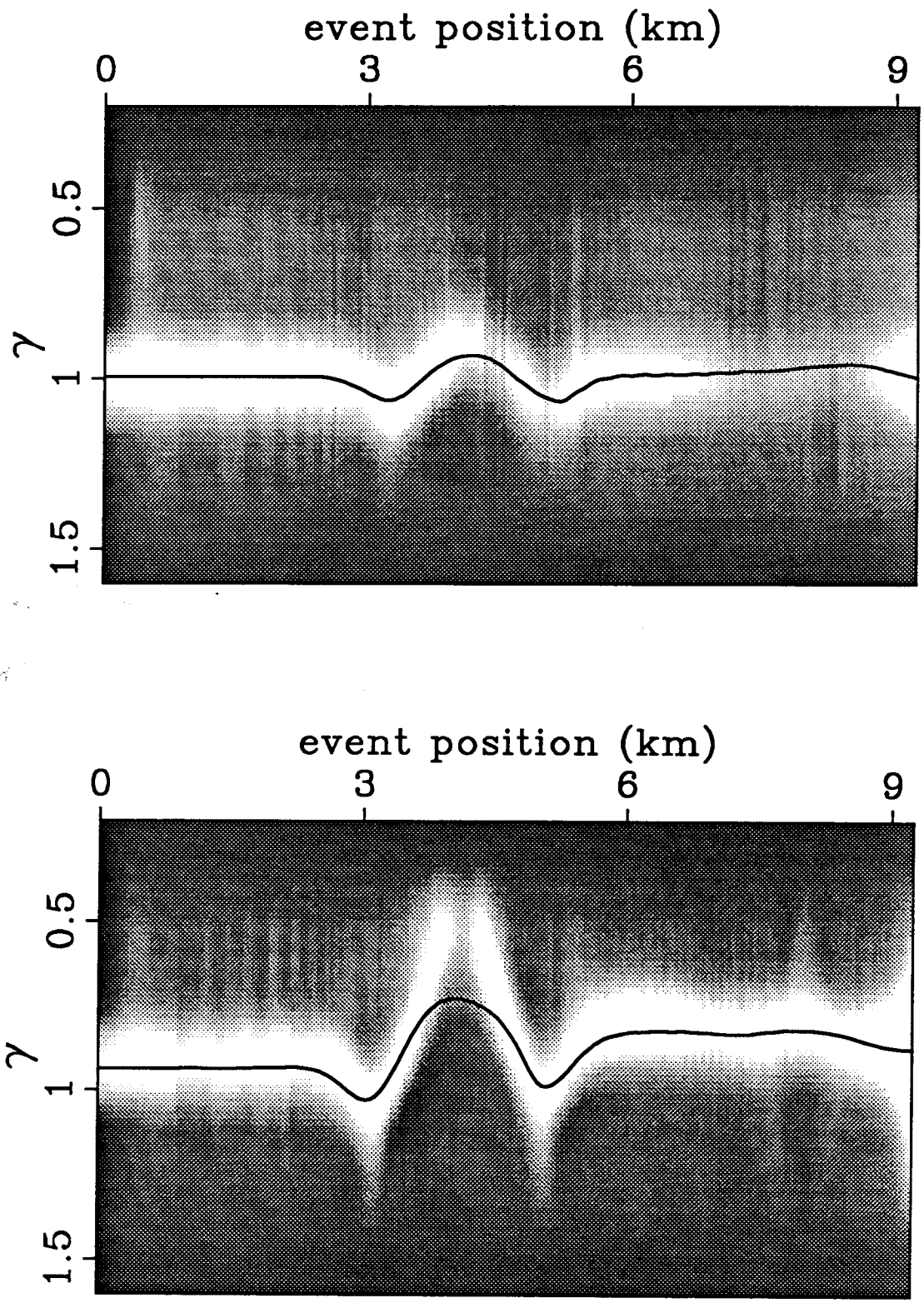

FIG. 3.20. Horizon residual-slowness analyses for the two reflectors in the image of Figure 3.19. The upper and lower gray-scale plots show semblance versus position and residual slowness γ for the upper and lower reflector respectively. The overlying dark lines on the semblance plots are the predicted values of γ.